

Spin torque nano-oscillators with a perpendicular spin polarizer

Cuixiu Zheng(郑翠秀), Hao-Hsau Chen(陈浩轩), Xiangli Zhang(张祥丽), Zongzhi Zhang(张宗芝), Yaowen Liu(刘要稳)

Citation: Chin. Phys. B . 2019, 28(3): 037503. **doi:** 10.1088/1674-1056/28/3/037503
Journal homepage: http://cpb.iphy.ac.cn; http://iopscience.iop.org/cpb

What follows is a list of articles you may be interested in

Dynamic nucleation of domain-chains in magnetic nanotracks

Xiangjun Jin(金香君), Yong Li(李勇), Fusheng Ma(马付胜)

Chin. Phys. B . 2018, 27(12): 127504. **doi:** 10.1088/1674-1056/27/12/127504

Realization of artificial skyrmion in CoCrPt/NiFe bilayers

Yi Liu(刘益), Yong-Ming Luo(骆泳铭), Zheng-Hong Qian(钱正洪), Jian-Guo Zhu(朱建国)

Chin. Phys. B . 2018, 27(12): 127503. **doi:** 10.1088/1674-1056/27/12/127503

Interfacial effect on the reverse of magnetization and ultrafast demagnetization in Co/Ni bilayers with perpendicular magnetic anisotropy

Zi-Zhao Gong(弓子召), Wei Zhang(张伟), Wei He(何为), Xiang-Qun Zhang(张向群), Yong Liu(刘永), Zhao-Hua Cheng(成昭华)

Chin. Phys. B . 2018, 27(5): 057501. **doi:** 10.1088/1674-1056/27/5/057501

Effects of dipolar interactions on magnetic properties of Co nanowire arrays

Hong-Jian Li(李洪健), MingYue(岳明), Qiong Wu(吴琼), Yi Peng(彭懿), Yu-Qing Li(李玉卿), Wei-Qiang Liu(刘卫强), Dong-Tao Zhang(张东涛), Jiu-Xing Zhang(张久兴)

Chin. Phys. B . 2017, 26(11): 117503. **doi:** 10.1088/1674-1056/26/11/117503

Faster vortex core switching with lower current density using three-nanocontact spin-polarized currents in a confined structure

Hua-Nan Li(李化南), Zhong Hua(华中), Dong-Fei Li(李东飞)

Chin. Phys. B . 2017, 26(1): 017502. **doi:** 10.1088/1674-1056/26/1/017502

SPECIAL TOPIC — Spin manipulation in solids

Spin torque nano-oscillators with a perpendicular spin polarizer*

Cuixiu Zheng(郑翠秀)[1], Hao-Hsau Chen(陈浩轩)[2], Xiangli Zhang(张祥丽)[2], Zongzhi Zhang(张宗芝)[2], and Yaowen Liu(刘要稳)[1,†]

[1] *Shanghai Key Laboratory for Special Artificial Microstructure Materials and Technology, School of Physics Science and Engineering, Tongji University, Shanghai* 200092, *China*

[2] *Department of Optical Science and Engineering, Fudan University, Shanghai* 200433, *China*

(Received 8 January 2019; revised manuscript received 25 January 2019; published online 26 February 2019)

We present an overview in the understanding of spin-transfer torque (STT) induced magnetization dynamics in spin-torque nano-oscillator (STNO) devices. The STNO contains an in-plane (IP) magnetized free layer and an out-of-plane (OP) magnetized spin polarizing layer. After a brief introduction, we first use mesoscopic micromagnetic simulations, which are based on the Landau–Lifshitz–Gilbert equation including the STT effect, to specify how a spin-torque term may tune the magnetization precession orbits of the free layer, showing that the oscillator frequency is proportional to the current density and the z-component of the free layer magnetization. Next, we propose a pendulum-like model within the macrospin approximation to describe the dynamic properties in such type of STNOs. After that, we further show the procession dynamics of the STNOs excited by IP and OP dual spin-polarizers. Both the numerical simulations and analytical theory indicate that the precession frequency is linearly proportional to the spin-torque of the OP polarizer only and is irrelevant to the spin-torque of the IP polarizer. Finally, a promising approach of coordinate transformation from the laboratory frame to the rotation frame is introduced, by which the nonstationary OP magnetization precession process is therefore transformed into the stationary process in the rotation frame. Through this method, a promising digital frequency shift-key modulation technique is presented, in which the magnetization precession can be well controlled at a given orbit as well as its precession frequency can be tuned with the co-action of spin polarized current and magnetic field (or electric field) pulses.

Keywords: spin torque nano-oscillators (STNOs), spin-transfer torque effect, magnetic simulation

PACS: 75.78.Cd, 85.70.Ay, 75.30.Ds **DOI:** 10.1088/1674-1056/28/3/037503

1. Introduction

Since the discovery of the spin-transfer torque (STT) effect by Slonczewski[1] and Berger,[2] an efficient manipulation of magnetization orientation has been achieved by applying a DC current perpendicularly to a sandwiched magnetic structure that consists of two magnetic layers separated by a nonmagnetic spacer.[3,4] The current first is polarized by the fixed magnetic layer and subsequently transfers the spin angular momentum to the free magnetic layer. The STT can act as negative damping, which can be used to switch the magnetization state of magnetic tunnel junctions (MTJs) and develop the so-called STT-MARM.[5,6] Another particularly important application of STT effect is to develop a new type of nanoscale microwave oscillators, called spin torque nano-oscillators (STNOs),[7,8] in which a persistent magnetization precession is required by controlling the STT strength to compensate the intrinsic Gilbert damping. Experimentally, the STNOs can be fabricated in the form of $\sim$ 100 nm diameter nanopillars[9] or in the form of a nanocontact on the top of a free layer, where the active magnetic layers are laterally extended over several micrometers.[10] The magnetization precession of STNOs can be uniform,[9] vortex mode,[11] or droplet mode.[12–15]

One of the qualities of STNOs is that they are tunable over a wide frequency range by varying the applied DC current or magnetic field. However, STNOs with a large microwave emission power and a narrow linewidth are of the most challenging issues to move the STNOs to the practical applications. The output power is typically in several to tens of pico-Watts or nano-Watt,[9,16,17] which is too weak for any practical applications. In order to improve the output power, several methods have been proposed, for example, using synchronization technique through the phase-locking mode of an array of STNOs[18–29] or using MgO-based MTJs to replace the spin valves,[30–32] which could increase the output power to several μW level because of an increased magnetoresistance signal.

However, most practical applications require these devices to operate in either zero or weak applied magnetic fields. For that, one particularly promising STNO device has been proposed by using a spin-torque nanopillar that consists of an out-of-plane (OP) magnetized spin polarizer and an in-plane (IP) magnetized free layer.[33–35] Another type of STNOs uses

*Project supported by the National Basic Research Program of China (Grant No. 2015CB921501) and the National Natural Science Foundation of China (Grant Nos. 11774260, 51671057, and 11874120).

†Corresponding author. E-mail: yaowen@tongji.edu.cn

© 2019 Chinese Physical Society and IOP Publishing Ltd

CoFeB-MgO based MTJ that consists of an OP free layer and an IP spin polarizer, which shows large-power microwave oscillations in the absence of any external magnetic fields.[36,37] The resonance modes of the free layer and reference layer have been recently identified by spin-torque ferromagnetic resonance (ST-FMR) technique.[38] In these two types of STNO geometries, since the spin-polarizing layer is perpendicular to the free layer in an $\sim 90^\circ$ magnetization configuration, a large spin-torque can be initially generated,[1] which would result in a lower threshold current to drive the OP precession and a larger amplitude of the microwave signals.

Another concern of the STNOs is to improve their linewidth.[39] Most of the oscillator linewidth comes from phase noise, which can be reduced by phase-locking[40] or non-conservative current-induced coupling between magnetic layers.[41] It also has been reported that the linewidth shows nonmonotonic temperature dependence as well as the nonlinearity of the devices.[38,42] Recently, a scheme for STNO-based modulation utilizing frequency shift keying (FSK)[43,44] or amplitude shift keying (ASK)[45] provides a new way to circumvent the issue of large linewidth. Digital data signals are employed by this modulation scheme without the requirement of radio-frequency (RF) mixer in demodulation. The data can be encoded by two distinct frequencies or two distinct oscillation amplitudes. In this paper, we will introduce an FSK modulation method by using the STNO with a perpendicular spin polarizer. By applying properly cooperative current and magnetic field pulses, we show that magnetization oscillation can be tuned at an OP precession orbit with a fixed tilted angle of magnetization (i.e., a fixed m_z) but with tunable frequencies.

The paper is organized as follows: In Section 2, the fundamental properties of the STNO with an OP spin polarizer are introduced. Then we show a pendulum-like theory model to describe such type of STNOs in Section 3. After that, the dynamics of STNOs with OP and IP dual spin-polarizers are further investigated in Section 4. In Section 5, a digital FSK technique is proposed. Finally, we give a brief summary in the end of the paper.

2. The STNOs with perpendicular spin polarizer

We consider a STNO device with a fixed OP polarizer and an in-plane magnetized free layer, as illustrated in Fig. 1(a). The separate nonmagnetic layer (NM1) between them can be a Cu metal for spin valves or a MgO insulating layer for MTJs in experiments. The magnetization dynamics of the free layer is governed by the Landau–Lifshitz–Gilbert (LLG) equation with additional spin-transfer torque terms[46]

$$\frac{\mathrm{d}\boldsymbol{M}}{\mathrm{d}t} = -\gamma(\boldsymbol{M}\times\boldsymbol{H}_{\mathrm{eff}}) + \frac{\alpha}{M_{\mathrm{s}}}\left(\boldsymbol{M}\times\frac{\mathrm{d}\boldsymbol{M}}{\mathrm{d}t}\right) + \frac{\gamma a_J}{M_{\mathrm{s}}}\boldsymbol{M}\times(\boldsymbol{M}\times\boldsymbol{p}) - \gamma b_J\boldsymbol{M}\times\boldsymbol{p}, \quad (1)$$

where $\boldsymbol{M} = m M_{\mathrm{s}}$ is the magnetization vector of the free layer, $\boldsymbol{m}$ is the unit magnetization vector, M_{s} is the saturation magnetization, $\boldsymbol{H}_{\mathrm{eff}}$ is the effective field that includes the external magnetic field, anisotropy field, demagnetizing field, exchange field, and dipolar field generated by the OP magnetic polarizer, and γ is the gyromagnetic constant. The first term of the LLG equation describes the Larmor precession of magnetization, the second term is the Gilbert damping term, α is the damping factor. The third and fourth terms are the in-plane Slonczewiski's spin torque[1] and field-like spin torque,[47–49] respectively. $\boldsymbol{p}$ is the unit magnetization vector of the polarizer layer, and a_J and b_J are the torque factors, $a_J = \hbar J g(P,\theta)/(2e\mu_0 M_{\mathrm{s}} d)$, $b_J = \xi a_J$. Here $\hbar$ is the Planck constant, J is the electric current density, d is the free layer thickness, e is the electron charge, P is the spin polarization, and $g(P,\theta)$ is the spin-torque efficiency factor from Slonczewski,[1] $g(P,\theta) = [-4+(1+P)^3(3+\cos\theta)/(4P^{3/2})]^{-1}$. $\xi = l_{\mathrm{ex}}/l_{\mathrm{sf}}$, which denotes the ratio of spin decoherence length and spin-flip relaxation length.[47] Here the thermal and multiple refection effect of STT[50] is ignored.

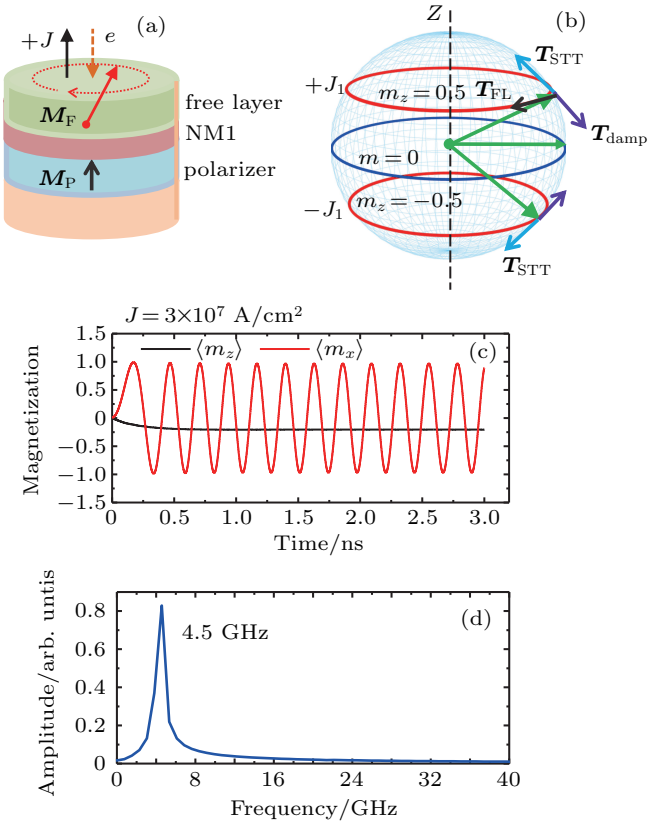


Fig. 1. (a) Schematic of a STNO with an in-plane magnetized free layer $\boldsymbol{M}_{\mathrm{F}}$ and a perpendicular spin polarizer $\boldsymbol{M}_{\mathrm{P}}$. The positive current J supports the parallel configuration of $\boldsymbol{M}_{\mathrm{F}}$ and $\boldsymbol{M}_{\mathrm{P}}$, which is defined as the current flowing from the free layer to the polarizer layer. (b) Schematic of STT-driven OP magnetization precession orbit, which is dependent of the applied current direction and amplitude. The blue arrow and black arrow indicate the Slonczewisk's torque ($\boldsymbol{T}_{\mathrm{STT}}$) and field-like spin torque ($\boldsymbol{T}_{\mathrm{FL}}$), respectively. The purple arrow denotes the damping torque. Panels (c) and (d) show the simulated typical magnetization precession and the corresponding oscillation frequency, respectively.

The free layer magnetization precession around z-axis stems from the current induced STT with the OP polarizer: the flow of incoming spin-polarized electrons tends to drag the free layer magnetization slightly out-of-plane. This yields the onset of a large perpendicular demagnetizing field around which the magnetization of the soft layer precesses. Depending on the current direction, the in-plane Slonczewiski's STT term in Eq. (1) can generate a torque either being parallel to the Gilbert damping torque or antiparallel to the damping torque (i.e., anti-damping torque), which can increase or decreases the Gilbert damping. In the anti-damping case, when the STT is smaller than the Gilbert damping, the magnetization precession is quickly damped and the magnet settles into static equilibrium.[51] In contrast, when the spin torque is larger than the damping torque, the precession increases until the magnetization completely reverses direction, which is usually used as the writing process for STT-MRAM. In the middle case, when the spin torque and the damping torque are effectively equal and opposite over a precession orbit, as shown in Fig. 1(b), a persistent magnetization precession will be observed. The precession orbit position (i.e., θ in the unit sphere phase plane) depends on the current direction and strength.

Figure 1(c) shows a typical time-dependent magnetization precession of the free layer excited by STT, and figure 1(d) shows the corresponding frequency calculated from the evolution of $\langle m_x \rangle$ with the fast Fourier transform (FFT) technique. In this simulation, the typical material parameters of permalloy ($Ni_{80}Fe_{20}$) are used for the free layer: $M_s = 800$ emu/cm^3 (saturation magnetization), $K = 5000$ erg/cm^3 (magnetic anisotropy), $A = 10^{-6}$ erg/cm^2 (exchange stiffness), $\alpha = 0.01$ (damping factor), and $P = 0.35$ (spin polarization). The lateral dimension of the free layer is 80 nm $\times$80 nm and the thickness $d = 4.5$ nm. The sample is descritized into a two-dimensional array of mesh cells in our simulations and each cell is 4 nm$\times$4 nm$\times$4.5 nm.

The critical current density for magnetic excitations can be derived from an instability condition of the OP component magnetization (M_z) within a single domain assumption[52,53]

$$J_c = \frac{2e}{\hbar} \frac{M_s \cdot d}{g(\theta = \pi/2)} \frac{H_K}{2}, \tag{2}$$

where H_K is the magnetic anisotropy field. The precession frequency (f) for a given current is given by

$$f = \frac{\gamma a_J}{2\pi\alpha} = \frac{\gamma}{2\pi\alpha} \frac{\hbar}{2e} \frac{g(\theta)}{M_s \cdot d} J. \tag{3}$$

Equation (2) indicates a linear dependency of the critical current density on the anisotropy field of the free layer. For our sample, the theoretically predicated J_c by Eq. (2) is 3.35×10^6 A/cm^2. The critical current could be reduced by optimizing the device geometry and parameters. For example, by decreasing the free layer thickness or increasing the spin polarization, we have $J_c = 1.19 \times 10^6$ A/cm^2 for $d = 1.6$ nm and $P = 0.35$ and $J_c = 6.79 \times 10^5$ A/cm^2 for further increased $P = 0.56$. These J_c values are close to that reported in Ref. [36].

Figure 2 shows the simulated oscillation frequency (solid triangles) as a function of the applied current. When the current density increases from 2×10^7 A/cm^2 to 1×10^8 A/cm^2, the frequency varies from 2 GHz to 13 GHz. We find that the frequency behavior strongly depends on the variation of the z-component of the averaged magnetization (open-circles), showing that the frequency is related to the effective demagnetization field of the free layer[53,54]

$$f = \frac{\gamma}{2\pi} 4\pi M_s \langle m_z \rangle. \tag{4}$$

Since the maximum demagnetizing field occurs when the magnetization of the free layer is driven fully perpendicular, the maximum precession frequency is $f_{max} = 2\gamma M_s = 28$ GHz. Simulations shown in Fig. 2 indicate that a flat plate at frequency of 6.8 GHz is observed for current density ranging from $(0.5–0.7)\times10^8$ A/cm^2, we infer that this comes from the competition between the demagnetization field (prefer to in-plane magnetization) and spin-transfer torque (prefer to $-z$ magnetization direction at positive current).

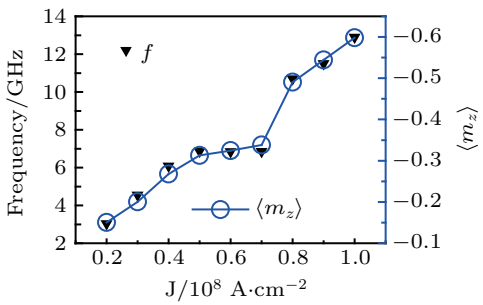


Fig. 2. Simulated OP precession frequency (left axis) and z-component of magnetization (right axis) as a function of the applied current density.

3. A pendulum-like theory model

In order to gain insight into the mechanism of STNOs with the perpendicular spin polarizer, Ebels *et al.* have presented a quite comprehensive description by using a generalized FMR formalism.[53] The work focuses on the in-plane bias field and the current-field phase diagram is well established through the theoretical model. Slavin *et al.* haves developed a general theoretical model for the STNOs via the nonlinear transformation of variables,[42] in which the LLG equation with STT effect has been exactly transformed into so-called universal model of an auto-oscillator with negative damping. However, the model becomes very complicated for the magnetization precession near the film in-plane, especially in the asymmetric case where the in-plane uniaxial anisotropy is taken into account to destroy the axial symmetry around z-axis.

Recently, we have developed an analytical pendulum-like model to describe the dynamics of STNO that contains an OP

polarizer combined with an IP free layer.[55] First, let us review a simple gravity pendulum model in classical mechanics, as shown in Fig. 3(a). When the pendulum is displaced sideways from its equilibrium position, it is subject to a restoring force due to gravity that will accelerate it back toward the equilibrium position. Consequently, the pendulum will oscillate about the equilibrium position, swinging back and forth. The potential energy for this harmonic oscillator is given by $V(\psi) = -mgl\cos\psi$, where m is the pendulum mass, l is the rod length, g is the gravitational acceleration, and ψ is the angle deviated from the equilibrium position. If an additional driving force $F_{\rm dri}$ is applied to the gravity pendulum along the tangential direction, the differential equation governing this gravity pendulum reads

$$\frac{{\rm d}^2\psi}{{\rm d}t^2} + \frac{g}{l}\sin\psi = \frac{1}{ml}F_{\rm dri}. \tag{5}$$

In the presence of driving force $F_{\rm dri}$, the pendulum could form a circling motion by tuning the driving force (bottom panel in Fig. 3(a)). In this case, the pendulum system is non-conservative and it could gain energy from the driving force.

We introduce this idea into the LLG equation to describe the oscillation dynamics of STNOs driven by the current-induced STT effect. In the absence of the field-like STT effect, the LLG equation is given by[56]

$$\begin{aligned}\frac{{\rm d}\boldsymbol{m}}{{\rm d}\tau} &= -(\nabla_{\boldsymbol{m}}E_{\rm T})\times\boldsymbol{m} + \alpha\left(\boldsymbol{m}\times\frac{{\rm d}\boldsymbol{m}}{{\rm d}\tau}\right)\\ &\quad + a_J\left[\boldsymbol{m}\times(\boldsymbol{m}\times\boldsymbol{p})\right].\end{aligned} \tag{6}$$

Here $a_J = A_J(\boldsymbol{m})(4\pi M_{\rm s}\gamma)^{-1}$ is the scaled STT strength with $A_J(\boldsymbol{m}) = (\gamma\hbar J/2eM_{\rm s}d)f(\boldsymbol{m}\cdot\boldsymbol{p})$ and $f(\boldsymbol{m}\cdot\boldsymbol{p}) = [-4 + C(P)(3+\boldsymbol{m}\cdot\boldsymbol{p})]^{-1}$, $C(P) = (1+P)^3/4P^{3/2}$. The total energy density scaled by $E_{\rm T}(\boldsymbol{m}) \equiv E(\boldsymbol{m})(4\pi M_{\rm s}^2)^{-1}$ can be rewritten in the two spherical angles of (θ, ϕ) as

$$E_{\rm T}(\theta,\phi) = \frac{1}{2}\cos^2\theta + \frac{k}{2}\sin^2\theta\sin^2\phi - h_z\cos\theta, \tag{7}$$

where the first term is the demagnetization energy density, the second term is the uniaxial anisotropic energy density, and the third one is the Zeeman energy density with a scaled magnetic field $h_z \equiv H_z/(4\pi M_{\rm s})$. The magnetic field is along $+z$ direction, which can comes from the stray field of the OP polarizer or the applied magnetic field. Consider that the order of the uniaxial anisotropy field is much smaller than that of the demagnetization field strength, e.g., $k = 0.008 \ll 1$, one can obtain a non-conservative Newton-like motion equation in the appearance of the damping and STT effect as (for details, see Appendixes A and B in Ref. [55])

$$\begin{aligned}&\ddot{\phi} + \sin^2\theta_0\alpha\dot{\phi}\\ &= -\frac{\sin^2\theta_0 a_{J0}}{-4+C(P)(3+\cos\theta_0)} - \frac{k}{2}\sin^2\theta_0\sin 2\phi.\end{aligned} \tag{8}$$

The precession inclination angle satisfies $\cos\theta_0 = h_z$.

Equation (8) is a typical damped nonlinear oscillator with a driving force by the action of STT effect. In the theory framework, the total effective force can be separated as the conservative ($F_{\rm con}$) and non-conservative terms ($F_{\rm non}$)

$$F_{\rm eff} = F_{\rm con} + F_{\rm non}. \tag{9}$$

For the local oscillations of the pendulum, the STT can be treated as a conservative-like force

$$F_{\rm con} = -(k/2)\sin 2\phi\sin^2\theta_0 - \frac{a_{J0}\sin^2\theta_0}{(-4+C(P)(3+\cos\theta_0))}, \tag{9a}$$

$$F_{\rm non} = -\sin^2\theta_0\alpha\dot{\phi}. \tag{9b}$$

In this case, the energy for the conservative system reads

$$\begin{aligned}E &= \frac{1}{2}\dot{\phi}^2 + V(\phi)\\ &= \frac{1}{2}\dot{\phi}^2 + \frac{k}{2}\sin^2\theta_0\cos^2\phi + \frac{a_{J0}\sin^2\theta_0\phi}{(-4+C(P)(3+\cos\theta_0))}.\end{aligned} \tag{10}$$

As for the rotation of the pendulum around the pivot, the STT can be treated as a non-conservative-like force

$$F_{\rm con} = -(k/2)\sin 2\phi\sin^2\theta_0, \tag{11a}$$

$$F_{\rm non} = -\sin^2\theta_0\left[\alpha\dot{\phi} + \frac{a_{J0}}{(-4+C(P)(3+\cos\theta_0))}\right]. \tag{11b}$$

Accordingly, the energy law becomes

$$E = \frac{1}{2}\dot{\phi}^2 + V(\phi) = \frac{1}{2}\dot{\phi}^2 + \frac{k}{2}\sin^2\theta_0\cos^2\phi. \tag{12}$$

In the first case, the STT effect is considered as a conservative-like driving force. The threshold of the STT strength to trigger an OP precession state can be derived,[55] which is independent of the damping constant

$$|a_{J0{\rm c}}| = (k/2)\left(-4+C(P)(3+\cos\theta_0)\right), \tag{13}$$

and the critical driving current is accordingly derived as

$$|I_{\rm c}| = \left(\frac{8\pi eM_{\rm s}^2V}{\hbar}\right)\left(\frac{k}{2}\right)\left(-4+C(P)(3+h_z)\right). \tag{14}$$

In the second case that the STT effect is considered as a non-conservative driving force, one will obtain another critical current $I_{\rm b}$, which corresponds to the lower boundary for OP precessions

$$\begin{aligned}|I_{\rm b}| &= \left(\frac{8\pi eM_{\rm s}^2eV}{\hbar}\right)\left(\frac{4\alpha}{2\pi}\right)\sqrt{k(1-h_z^2)}\\ &\quad\times\left[-4+C(P)(3+h_z)\right].\end{aligned} \tag{15}$$

Note that $I_{\rm b}$ in Eq. (15) is proportional to the Gilbert damping constant α, which definitely implies that for a larger damping the more driving current is required to compensate the energy loss to maintain an OP precession trajectory. Figure 3(b) shows the phase diagram of these two critical currents of $I_{\rm b}$ and $I_{\rm c}$ with three stable coexisting states containing the

quasi-static parallel (P), antiparallel (AP), and OP precessions. The two stable P and AP states appear for the current smaller than I_b. Theoretically predicted I_c and I_b are calculated from Eqs. (14) and (15), respectively, as a function of magnetic field h_z. Meanwhile, the critical currents obtained by the macrospin simulation are also given by the blue-squares and open-circles. Note that the critical currents linearly increase with the increase of h_z, showing a good agreement between the theory and simulations. Figure 3(c) shows that two typical clockwise OP precession states appear for any initial magnetization state when the applied current is taken the values a little above I_c (the stars in Fig. 3(b)). These results clearly indicate that the STNOs with the perpendicular polarizer can be well treated as a pendulum-like oscillator, in which the non-conservative STT effect behaves for the out-of-plane magnetization precessions.

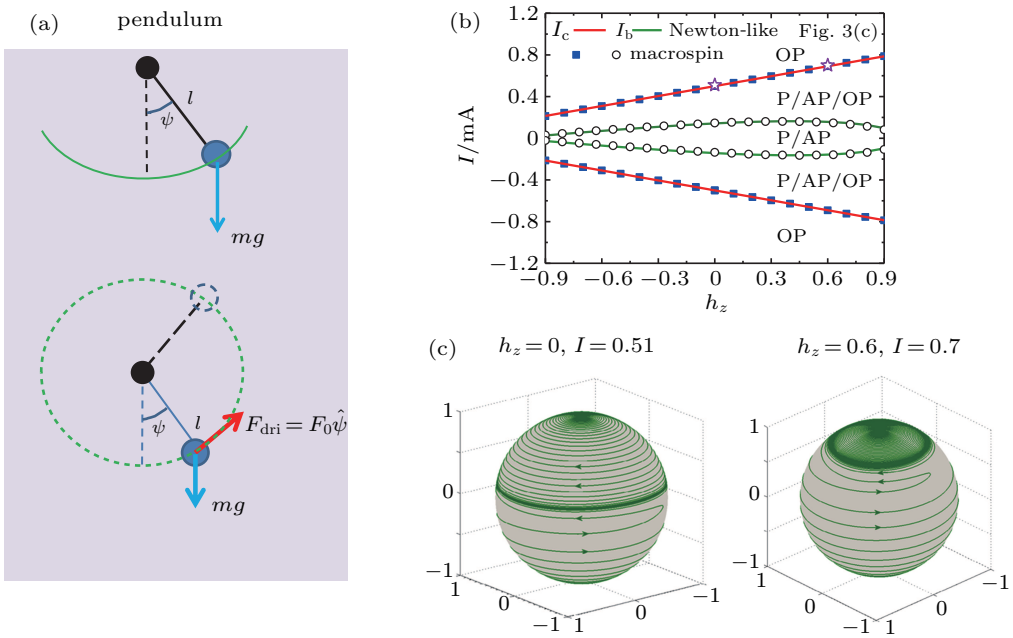


Fig. 3. (a) Schematic pendulum models in the uniform gravity and driven by a tangential force. (b) The phase diagrams of the static and oscillation free layer magnetization states as functions of current and field. The theory predications of the critical currents I_c and I_b for OP precession are indicated by red and olive curves, respectively. The corresponding simulation results are indicated by the blue and black squares. P and AP denote the parallel state and antiparallel state with respective to the IP analyzer, respectively. (c) Simulated OP magnetization precession of the free layer on the unit sphere phase plane for two combinations of currents I and applied fields h_z.

4. STNO with dual spin polarizers

One of the key attractions in the STNO with perpendicular polarizer and in-plane free layer is that the orthogonal magnetization configuration could generate a large STT in the initial stage. This can be used to solve the unavoidable intrinsic drawback in such devices that spin-toque is almost zero at the initial stage when the two layer magnetizations are collinearly aligned, which usually results in the relatively long incubation period of switching time. For that, STT nanopillars with dual spin-polarizing layers have attracted much attention.[57] As illustrated in Fig. 4(a), one spin-polarizing layer is magnetized in-plane (referred to as IP polarizer) and the other is magnetized out-of-plane (referred to as OP polarizer). Recent experiments have demonstrated that the combined IP and OP dual polarizers could significantly enhance the spin-torque effect, increase the magnetization switching speed, and lower the pulse width by a factor of 10, as compared with the devices with a single IP polarizer.[58–61] Our previous simulations show that ultrashort current pulses down to 150 ps even can drive the free layer magnetization switching.[62]

The magnetization dynamics of the free layer can be described by the LLG equation including the two spin-torque terms generated from OP and IP dual polarizers, respectively

$$\frac{\mathrm{d}\boldsymbol{M}}{\mathrm{d}t} = -\gamma(\boldsymbol{M}\times\boldsymbol{H}_{\mathrm{eff}}) + \frac{\alpha}{M_s}\left(\boldsymbol{M}\times\frac{\mathrm{d}\boldsymbol{M}}{\mathrm{d}t}\right) + \frac{\gamma a^J_{\mathrm{OP}}}{M_s}\boldsymbol{M} \times(\boldsymbol{M}\times\boldsymbol{p}_{\mathrm{OP}}) - \frac{\gamma a^J_{\mathrm{IP}}}{M_s}\boldsymbol{M}\times(\boldsymbol{M}\times\boldsymbol{p}_{\mathrm{IP}}), \tag{16}$$

where the STT factor $a^J_{\mathrm{OP(IP)}} = (\hbar/2)(1/\mu_0 M_s)(1/t)(J/|e|)\times P_{\mathrm{OP(IP)}}g(\boldsymbol{M}\cdot\boldsymbol{p}_{\mathrm{OP(IP)}})$. In this study, the STT efficiency factor is taken as $g(\boldsymbol{M}\cdot\boldsymbol{p}) = [\cos^2(\varphi/2) + 1/(1+\chi)\sin^2(\varphi/2)]^{-1}$, with ϕ as the angle between $\boldsymbol{M}$ and $\boldsymbol{p}$, and χ is an asymmetric parameter.[63] For simplicity, here we ignore the asymmetric effect of STT and set $\chi = 0$.

First, the free layer magnetization switching in the film plane (from $-x$ to $+x$ switching) is tested by using the IP and OP dual polarizers. Macrospin simulation results shown

in Fig. 4(b) indicate that the switching time of the free layer can be significantly reduced in the spin-torque device with the IP and OP dual polarizers (red curve), as compared with that having a single IP polarizer (blue curve). In these two simulations, the applied current pulse strength is the same, $J = 7.94 \times 10^{11}$ A/m^2. The standard material parameters of CoFeB are used for the free layer: $\mu_0 M_s = 1.5$ T, $d = 5$ nm, $K = 1920$ J/m^3. The electron spin polarizations of the IP and OP polarizers are assumed to be 0.7 and 0.02, respectively. Note that, although the STT strength generated from the OP polarizer is very small ($a^J_{\rm OP}/a^J_{\rm IP} \simeq 0.028$), the free layer switching completes within ~ 0.7 ns, which is much faster than that in the single IP polarizer case (~ 8.7 ns).

Figure 4(c) summarizes the phase diagram of STNOs as a function of the STT strength from OP and IP dual polarizers. The magnetization behaviors can be categorized into three regions: (I) no switching, (II) switching, and (III) oscillation. In region-I, the two torques are not strong enough to switch the magnetization orientation of the free layer. In region-II, the two spin-torques could drive the free layer magnetization to switch from $-x$ to $+x$ direction, showing that the switching occurs when the STT strength from the OP polarizer $a^J_{\rm OP}$ is almost one order smaller than that from the IP polarizer $a^J_{\rm IP}$. The STT effect from the OP polarizer is very helpful in accelerating the speed of the magnetization switching. With the increase of $a^J_{\rm OP}$, the free layer magnetization enters region-III and displays a periodic OP precession state.

Interestingly, the periodic precession frequency of the free layer exhibits different feature dependence on the OP and IP polarizers, as shown in Fig. 4(d). At a fixed OP spin-torque of $a^J_{\rm OP} = 0.3 \times 10^4$ A/m, the precession frequency is ~ 9.8 GHz, which is almost independent of the torque strength generated by the IP polarizer. In contrast, for a given IP spin-torque, $a^J_{\rm IP} = 1.125 \times 10^4$ A/m, the frequency linearly increases with the increase of the OP spin-torque. This significant difference of frequency dependence on the torques reveals that the OP spin-torque plays an important role in the magnetization OP precessions. With the increase of the tilt angle of magnetization (and thereby, the z-component of magnetization), the precession accelerates and frequency increases. Such a frequency dependence on the tilt angle of magnetization is in agreement with Eq. (4).[54] We know that the tilt angle of magnetization in the device of Fig. 4(a) is mainly dominated by the OP spin-torque. Therefore, the frequency is almost unchanged at a fixed OP spin-torque case and increases with the increased OP spin-torque.

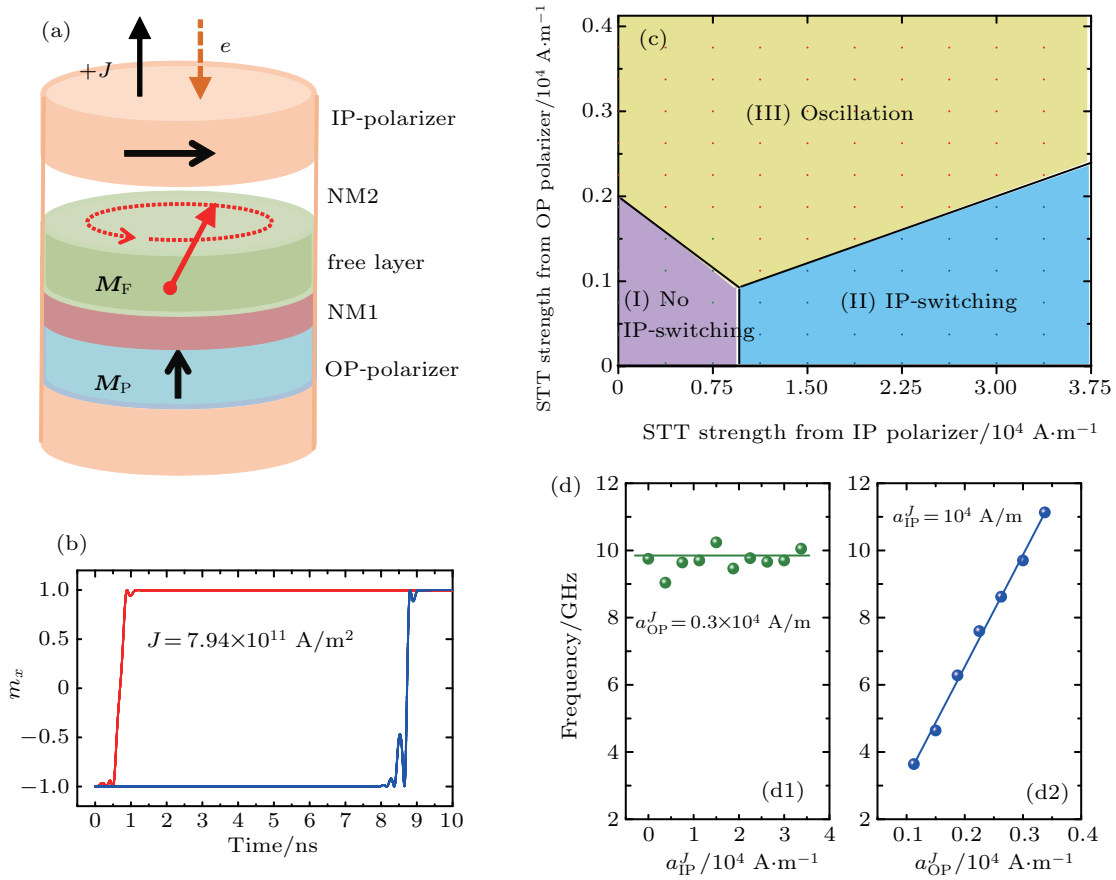


Fig. 4. (a) A schematic configuration of a STNO with IP and OP dual polarizers. (b) Comparison of magnetization switching driven by spin-torques excited by dual polarizers (red-curve) and by a single IP polarizer (blue-curve). (c) Phase diagram of the free layer magnetization dynamics dependence on the spin-torques strengths generated from the IP and OP polarizers. (d) Oscillation frequency dependence on the spin-torque strengths at a fixed OP spin-torque (a) and a fixed IP spin-torque.

To gain deep insights into the frequency characteristics of the STNO with dual polarizers, an analytical model has been developed.[62] In this device, the effective field acting on the free layer reads

$$\boldsymbol{H}_{\rm eff} = \left(H_{\rm k}\frac{M_x}{M_{\rm s}} - H_x\right)\boldsymbol{e}_x + (H_z - 4\pi M_z)\boldsymbol{e}_z, \tag{17}$$

where $H_{\rm k}$ is the intrinsic in-plane anisotropy field, and H_x and H_z are the stray fields generated from the IP and OP polarizers, respectively. The demagnetizing field is $-4\pi M_z$. By inserting Eq. (17) into Eq. (16), we obtain the following equation for the M_z component:

$$\begin{aligned}\frac{{\rm d}M_z}{{\rm d}t} &= \gamma M_y\left(H_{\rm k}\frac{M_x}{M_{\rm s}} - H_x\right) + \frac{\alpha}{M_{\rm s}}\left(M_x\frac{{\rm d}M_y}{{\rm d}t} - M_y\frac{{\rm d}M_x}{{\rm d}t}\right)\\ &\quad - \frac{\gamma a^J_{\rm OP}}{M_{\rm s}}(M_x^2 + M_y^2) - \frac{\gamma a^J_{\rm IP}}{M_{\rm s}}M_xM_z.\end{aligned} \tag{18}$$

Taking $\boldsymbol{M} = |\boldsymbol{M}_\perp|\cos(2\pi f\cdot t)\boldsymbol{e}_x + |\boldsymbol{M}_\perp|\sin(2\pi f\cdot t)\boldsymbol{e}_y + M_z\boldsymbol{e}_z$, here $\boldsymbol{M}_\perp$ is the in-plane component and f is the oscillation frequency, equation (18) can be rewritten as

$$\begin{aligned}\frac{{\rm d}M_z}{{\rm d}t} &= \frac{\gamma H_{\rm k}}{M_{\rm s}}|\boldsymbol{M}_\perp|^2\cos(2\pi f\cdot t)\sin(2\pi f\cdot t)\\ &\quad - \gamma H_x|\boldsymbol{M}_\perp|\sin(2\pi f\cdot t) + \frac{\alpha}{M_{\rm s}}|\boldsymbol{M}_\perp|^2 2\pi f\\ &\quad - \frac{\gamma a^J_{\rm OP}}{M_{\rm s}}|\boldsymbol{M}_\perp|^2 - \frac{\gamma a^J_{\rm IP}}{M_{\rm s}}|\boldsymbol{M}_\perp|\cos(2\pi f\cdot t)M_z.\end{aligned} \tag{19}$$

Consider that the change of M_z is very small in an precession period and by time-integrating both sides of Eq. (19) in a period of 2π, the oscillation frequency can be derived as

$$f \approx \frac{\gamma a^{\rm OP}_J}{2\pi\alpha} = \frac{\gamma}{2\pi\alpha}\frac{\hbar}{2|e|}\frac{P_{\rm OP}}{M_{\rm s}\cdot t}|J|. \tag{20}$$

Equation (20) clearly indicates that the precession frequency in this device is linearly proportional to the spin-torque of the OP polarizer only and is irrelevant to the spin-torque of the IP polarizer. This analytical result is in perfect agreement with the simulation results shown in Fig. 4(d).

5. Digital FSK modulation technique

As mentioned in Fig. 2(a),the magnetization precession orbit around z-axis in the local spherical coordinate frame can be controlled by the current strength. The precession frequency can be tuned from several to tens of GHz which is related to the changing of polar angle θ. As a result, different currents will drive the free layer magnetization precessing in the different orbits with the different frequencies, showing the increased frequency with the decrease of θ. Consequently, two distinct precession frequencies have two different magnetization oscillation amplitudes (thereby, different θ).

How to realize two distinct frequencies without any change of oscillation amplitudes is a key issue for frequency modulation (FM) application of STNOs in the wireless communications. This requires the free layer magnetization to rotate in a fixed precession orbit but with different precession frequency. Recently, a scheme for STNO-based modulation utilizing frequency shift keying (FSK) or amplitude shift keying (ASK) has been introduced,[45] in which the data can be encoded by two distinct frequencies or two distinct oscillation amplitudes, namely, the binary FSK or binary ASK technique, respectively. In this section, we will introduce two possible techniques of digital FSK modulation.

The first design uses the STT device as shown in Fig. 5(a), in which the STNO has the IP free layer and OP polarizer. A current pulse and a perpendicular magnetic field pulse h_z are applied to the nano-pillar. As mentioned before, the magnetization dynamics of the free layer can be described by the LLG equation with the STT effect given in Eq. (6).

In order to analyze the stability of magnetization dynamics, the model is transformed into a reference frame rotating at angular frequency ω around the symmetry z-axis. Thus, the time derivative of $m(\tau)$ in the frame transformation is given by

$$\left[\frac{{\rm d}\boldsymbol{m}}{{\rm d}\tau}\right]_{\rm lab} = \left[\frac{{\rm d}\boldsymbol{m}}{{\rm d}\tau}\right]_{\rm rot} + [\omega_z(m_z)\boldsymbol{z}]\times\boldsymbol{m}, \tag{21}$$

where lab and rot denote the laboratory frame and rotating frame, respectively. The angular frequency ω used here is dependent on the z-component of magnetization (i.e., the frame transformation is a local transformation). Accordingly, the LLG equation in the rotating frame reads

$$\begin{aligned}\left[\frac{{\rm d}\boldsymbol{m}}{{\rm d}t}\right]_{\rm rot} &= -[\nabla_{\boldsymbol{m}}E + \omega_z(m_z)\boldsymbol{z}]\times\boldsymbol{m} + \alpha\boldsymbol{m}\times\left[\frac{{\rm d}\boldsymbol{m}}{{\rm d}t}\right]_{\rm rot}\\ &\quad - [a_J(\theta) + \alpha\omega(m_z)]\,[\boldsymbol{m}\times(\boldsymbol{m}\times\boldsymbol{z})].\end{aligned} \tag{22}$$

Interestingly, owing to the coordinate transformation, there are two additional terms in the LLG equation generated in the rotating frame: the first one is the field-like torque $\boldsymbol{T}_1 = \omega_z(m_z)\boldsymbol{z}\times\boldsymbol{m} = \boldsymbol{h}_{\rm rot}\times\boldsymbol{m}$, which can be absorbed into the energy density term in the rotation frame in Eq. (20); the second term has the anti-STT like torque formula $\boldsymbol{T}_{\rm rot} = \alpha\omega_z(m_z)[\boldsymbol{m}\times(\boldsymbol{m}\times\boldsymbol{z})]$, whose strength depends on the damping and angular frequency. The $\boldsymbol{T}_{\rm rot}$ term can be combined with the STT terms of laboratory frame. Figure 5(b) illustrates the two newborn torque directions.

It is worth remarking that equation (22) implies that the original STT can be completely canceled by the anti-STT like torque when a proper rotation frame with a synchronous rotation frequency ω_z is chosen

$$a_J(\boldsymbol{m}) + \alpha\omega_z(m_z) = 0. \tag{23}$$

In this case, equation (22) in the rotation frame can be rewritten as

$$\left[\frac{{\rm d}\boldsymbol{m}}{{\rm d}t}\right]_{\rm rot} = -[\nabla_{\boldsymbol{m}}E_{\rm rot}]\times\boldsymbol{m} + \alpha\boldsymbol{m}\times\left[\frac{{\rm d}\boldsymbol{m}}{{\rm d}t}\right]_{\rm rot}, \tag{24}$$

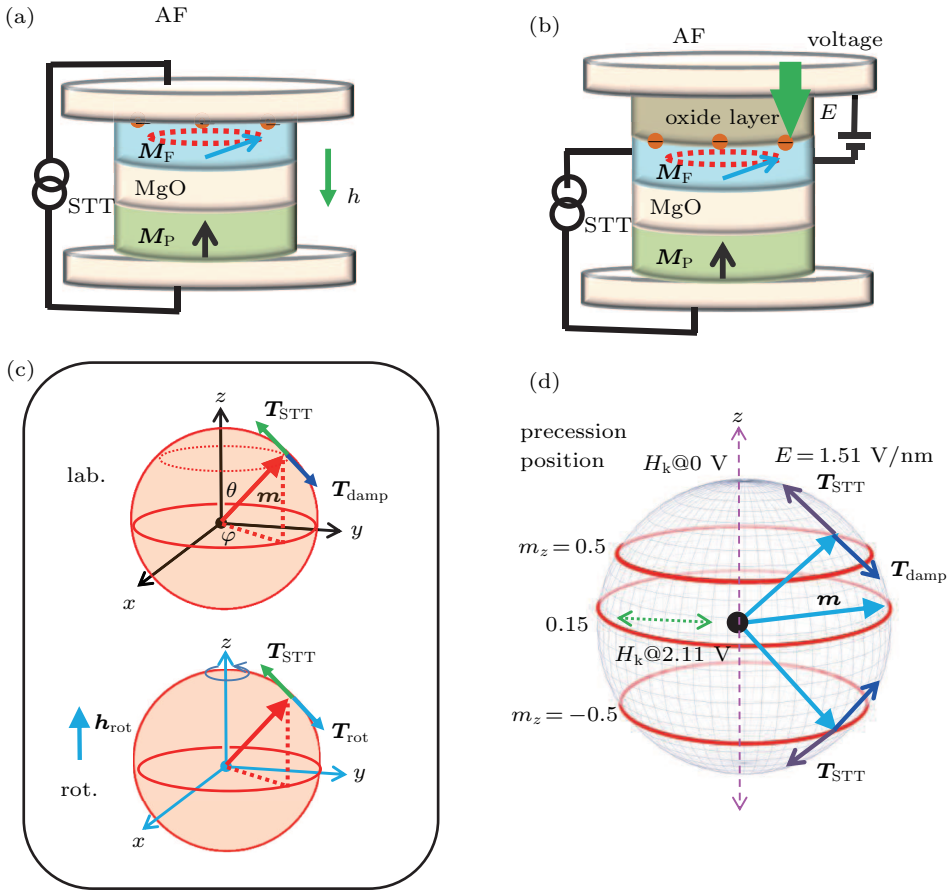


Fig. 5. (a) Schematic of a STNO-based FSK modulation scheme by current pulse $I(t)$ and magnetic field pulse $h_z(t)$. The free layer is in-plane magnetized free layer and the polarizer layer is perpendicularly magnetized. (b) Schematic of frame transformation for an OP magnetization precession in the laboratory inertia frame and in the rotating frame with an angular frequency ω, respectively. The green and blue arrows denote the damping and STT vectors, respectively. The cray arrow denotes the virtual torque vector due to the coordinate transformation. $\boldsymbol{h}_{\rm rot}$ is a virtual field along z-axis whose amplitude is associated to $\omega(m_z)$. Panels (c) and (d) show the E-field assisted FSK modulation scheme. Both the free layer and polarizer layer in the STNO have the perpendicular anisotropy. The additional oxide layer on the top of the free layer is used to apply the E-field and tunes the PMA.

with the effective total energy $E_{\rm rot}$,

$$E_{\rm rot}(m_z) = \frac{1}{2}m_z^2 - h_z m_z - \frac{a_{J0}}{\alpha C(P)}\ln\left[-4+C(P)(3+m_z)\right]. \quad (25)$$

Thus, the original STT effect of laboratory frame can be exactly transformed into one part of the total energy in Eq. (25).

By this way, an OP precession state at a given orbit of m_{z0} (z-component) can be treated as a static state in the rotating frame designated by m_{z0} and subjected to $(\mathrm{d}\boldsymbol{m}/\mathrm{d}t)_{\rm rot} = 0$. Thus, the stability of OP magnetization precession orbit at the fixed m_{z0} is derived from $\partial E_{\rm r}/\partial m_z = 0$ and $\partial^2 E_{\rm r}/\partial m_z^2 > 0$. It yields that the applied current and magnetic field should satisfy

$$I = \left(\frac{8\pi e M_{\rm s}^2 V}{\hbar}\right)(m_{z0}-h_z)\,\alpha\left[-4+C(P)(3+m_{z0})\right], \quad (26)$$

$$\left(\frac{\hbar}{8\pi e M_{\rm s}^2 V}\right)\frac{I}{\alpha}\frac{C(P)}{\left[-4+C(P)(3+m_{z0})\right]^2} > -1. \quad (27)$$

The precession frequency of the stable OP precession orbit can be analytically derived as

$$f(\mathrm{GHz}) = \frac{4\pi M_{\rm s}\gamma}{2\pi}\left|h_z - m_{z0}\right|. \quad (28)$$

Through Eqs. (24)–(26), a stable OP precession orbit with a controllable frequency can be realized by choosing a proper cooperation of current and magnetic field (I, h_z).

Figure 6 shows the simulation results by using two groups of current pulses alone ($I_0 = 0.1$ mA and $I_1 = 2$ mA). Clearly, in the case of current alone shown in Figs. 6(a)–6(c), the STT drives the free layer into two distinct precession orbits with different frequencies at 1.2 GHz and 17.8 GHz, respectively. But the different oscillation amplitudes in m_x are observed (Fig. 6(c)), which will actually generate different GMR signals.

The ideal digital FSK modulation requires a frequency modulation between two states but without any changes of magnetization oscillation amplitude. To achieve this goal, a proper cooperation scheme is applied by using two combinations of driving pulses (I_0, h_{z0}) and (I_1, h_{z1}) governed by Eqs. (26) and (27). The results are shown in Figs. 6(d)–6(f). As expected, the enhanced current I_1 drives the magnetization

precession orbit out of x–y plane to switch frequency to be f_1. Meanwhile, the negative magnetic field h_{z1} brings the magnetization toward the film plane to keep the magnetization oscillation amplitude, which causes the m_z decreasing back to m_{z0}. Consequently, the OP precession is stabilized on the same orbit with a fixed tilt angle ($m_z = 0$, thereby the same oscillation amplitudes of m_x and m_y) for the two combinations of driving pulses, (I_0, h_0) and (I_1, h_1). Meanwhile, the magnetization precession possesses two different frequencies, $f_0 = 0.5$ GHz and $f_1 = 2.0$ GHz, respectively. It can be used to code two different frequency modulation signals.

The controllable frequency modulation can also be done in the second design scheme, as illustrated in Fig. 5(b). By using the perpendicularly magnetized magnetic tunnel junction (MTJ), we show that the magnetization oscillation frequency can be tuned by the co-action of electric field and spin polarized current.[44] Both the fixed polarizer layer M_P and the free layer M_F are magnetized perpendicularly due to the strong perpendicular magnetic anisotropy (PMA). In this case, the positive current J supports the parallel configuration of M_F and M_P. The additional oxide layer is used to apply the E-field and accumulate electric charge on the free layer to tune its PMA. The OP precession can be stabilized at a given orbit with a fixed tilted angle of magnetization m_z but with a tunable frequency for the two combinations of driving pulses, (J_1, E_1) and (J_2, E_2). The frequency of precession satisfies

$$f = \frac{4\pi M_s \gamma}{2\pi}\left|-\frac{a_J}{\alpha}\right| = \left|2K_{S_i,\mathrm{eff}}(E)\, m_z\right| \frac{2M_s\gamma}{1+\alpha\xi}\frac{1}{2}. \tag{29}$$

Finally, we would like to point out that the FSK modulation can be done not only in a single device to switch the STNO into two frequency bands, but also can be realized in two and even more STNOs with the synchronized precession frequencies. The phase locking of multiple STNOs can be realized by an electrical circuit design[27] or magnetic dipolar coupling effect.[29,64]

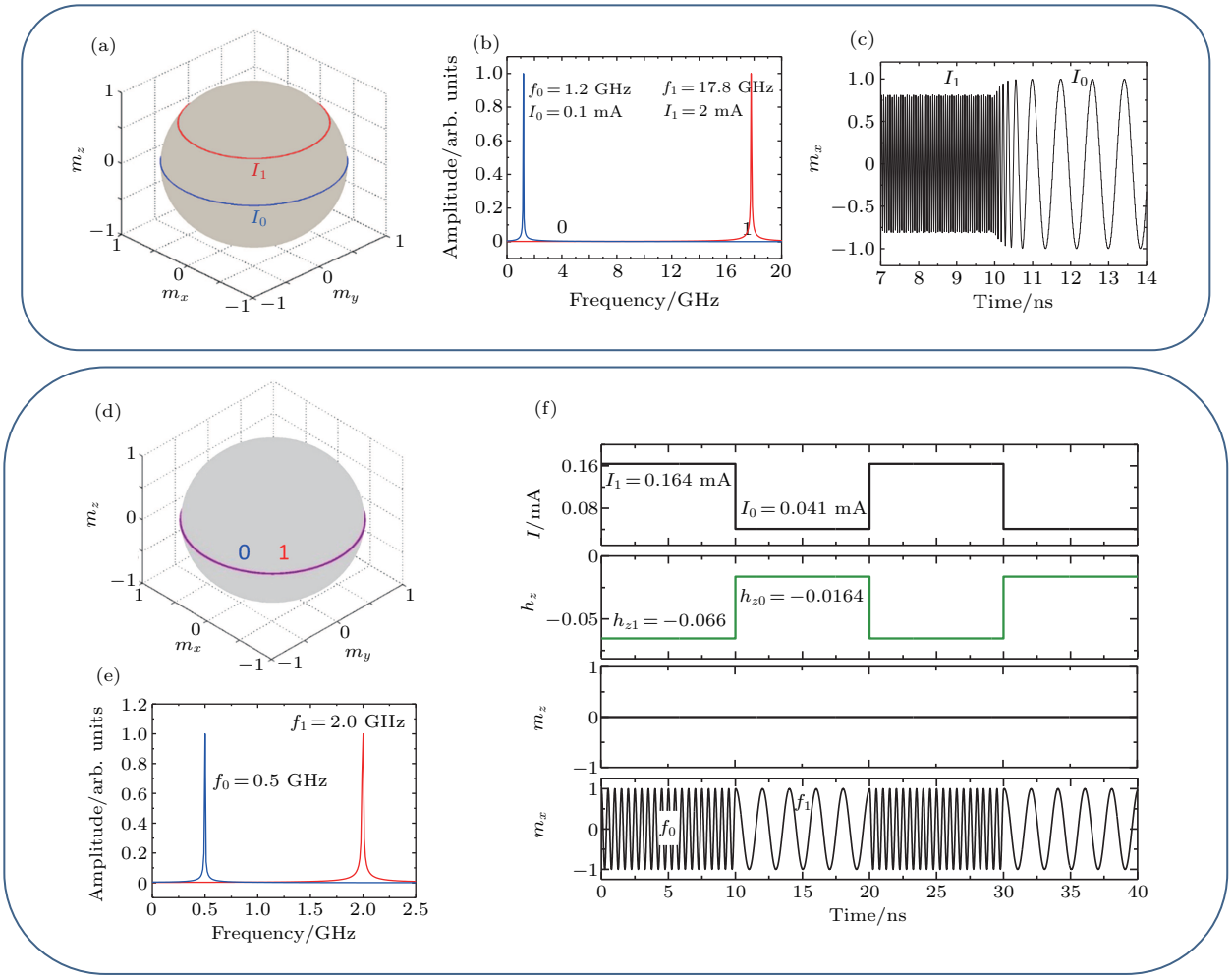


Fig. 6. (a)–(c) Digital FSK modulation based on PERP-STNO operated by current pulse only. (a) Magnetization precession trajectories at two current pulses of $I_0 = 0.1$ mA and $I_1 = 2$ mA, respectively. The pulse duration is 10 ns. (b) Frequency spectra of the two precession states calculated by FFT transformation. (c) The evolution of x-component of magnetization. (d)–(f) Digital FSK modulation implemented through the collaborative operation between the current and field pulses. The magnetization precessions are forced into the orbit with $m_z = 0$. (d) Magnetization precession trajectories at (I_1, h_{z1}) and (I_2, h_{z2}), corresponding to the bits "0" and "1", respectively. (e) The frequency spectra of the two precession states. (f) The time evolution of m_x and m_z response to the current and field pulses.

6. Conclusion

In summary, we have studied the dynamic properties of the STNOs with a perpendicular spin polarizer. A persistent OP magnetization precession appears when the spin torque and the damping torque are effectively equal and opposite over a precession orbit. The position of the precession orbit (i.e., θ in the unit sphere phase plane) depends on the current direction and strength, and the precession frequency is a function of the current strength as well as the θ angle. We show that the OP precession can be described as a pendulum-like oscillation model, in which the STT effect can be treated as the conservative and non-conservative terms. We also discuss the dynamics of STNOs with OP and IP dual spin polarizers and find that the OP precession frequency is mainly dominated by the OP polarizer. In the last part we show that the STNO with perpendicular polarizer can be used as a good candidate for the digital frequency shift-key modulation technique. The magnetization precession at a given orbit but with a tunable frequency can be realized by the co-action of magnetic field (or electric field) and spin polarized current. We expect this controllable frequency modulation can be used in the BFSK technique of wireless communication.

References

[1] Slonczewski J C 1996 *J. Magn. Magn. Mater.* **159** L1
[2] Berger L 1996 *Phys. Rev. B* **54** 9353
[3] Katine J A, Albert F J, Buhrman R A, Myers E B and Ralph D C 2000 *Phys. Rev. Lett.* **84** 3149
[4] Liu Y, Zhang Z, Freitas P P and Martins J L 2003 *Appl. Phys. Lett.* **82** 2871
[5] Slaughter J M, Rizzo N D, Janesky J, Whig R, Mancoff F B, Houssameddine D, Sun J J, Aggarwal S, Nagel K, Deshpande S, Alam S M, Andre T and LoPresti P 2012 *International Electron Devices Meeting,* December 10–13, 2012, San Francisco, CA, pp. 29.3.1–29.3.4
[6] Huai Y 2018 *AAPPS Bull.* **18** 33
[7] Silva T J and Rippard W H 2008 *J. Magn. Magn. Mater.* **320** 1260
[8] Chen T, Dumas R K, Eklund A, Muduli P K, Houshang A, Awad A A, Malm B G, Rusu A J and kerman 2016 *Proc. IEEE* **104** 1919
[9] Kiselev S I, Sankey J C, Krivorotov I N, Emley N C, Schoelkopf R J, Buhrman R A and Ralph D C 2003 *Nature* **425** 380
[10] Rippard W H, Pufall M R, Kaka S, Russek S E and Silva T J 2004 *Phys. Rev. Lett.* **92** 027201
[11] Pribiag V S, Krivorotov I N, Fuchs G D, Braganca P M, Ozatay O, Sankey J C, Ralph D C and Buhrman R A 2007 *Nat. Phys.* **3** 498
[12] Hoefer M A, Sommacal M and Silva T J 2012 *Phys. Rev. B* **85** 214433
[13] Mohseni S M, Sani S R, Persson J, Nguyen T N A, Chung S, Pogoryelov Y, Muduli P K, Iacocca E, Eklund A, Dumas R K, Bonetti S, Deac A, Hoefer M A and Åkerman J 2013 *Science* **339** 1295
[14] Xiao D, Liu Y, Zhou Y, Mohseni S M, Chung S and Åkerman J 2016 *Phys. Rev. B* **93** 094431
[15] Xiao D, Tiberkevich V, Liu Y H, Liu Y W, Mohseni S M, Chung S, Ahlberg M, Slavin A N, Åkerman J and Zhou Y 2017 *Phys. Rev. B* **95** 024106
[16] Deac A M, Fukushima A, Kubota H, Maehara H, Suzuki Y, Yuasa S, Nagamine Y, Tsunekawa K, Djayaprawira D D and Watanabe N 2008 *Nat. Phys.* **4** 803
[17] Ryo H, Hitoshi K, Sumito T, Shingo T, Kay Y, Akio F, Rie M, Hiroshi I and Shinji Y 2016 *Appl. Phys. Express* **9** 053006
[18] Kaka S, Pufall M R, Rippard W H, Silva T J, Russek S E and Katine J A 2005 *Nature* **437** 389
[19] Mancoff F B, Rizzo N D, Engel B N and Tehrani S 2005 *Nature* **437** 393
[20] Slavin A N and Tiberkevich V S 2006 *Phys. Rev. B* **74** 104401
[21] Pufall M R, Rippard W H, Russek S E, Kaka S and Katine J A 2006 *Phys. Rev. Lett.* **97** 087206
[22] Chen X and Victora R H 2009 *Phys. Rev. B* **79** 180402
[23] Tiberkevich V, Slavin A, Bankowski E and Gerhart G 2009 *Appl. Phys. Lett.* **95** 262505
[24] Ruotolo A, Cros V, Georges B, Dussaux A, Grollier J, Deranlot C, Guillemet R, Bouzehouane K, Fusil S and Fert A 2009 *Nat. Nanotech.* **4** 528
[25] Kendziorczyk T and Kuhn T 2016 *Phys. Rev. B* **93** 134413
[26] Houshang A, Iacocca E, Durrenfeld P, Sani S R, Akerman J and Dumas R K 2016 *Nat. Nanotech.* **11** 280
[27] Grollier J, Cros V and Fert A 2006 *Phys. Rev. B* **73** 060409
[28] Chen H, Chang J and Chang C 2011 *SPIN* **01** 1
[29] Chen H H, Lee C M, Zhang Z, Liu Y, Wu J C, Horng L and Chang C R 2016 *Phys. Rev. B* **93** 224410
[30] Zeng Z, Amiri P K, Krivorotov I N, Zhao H, Finocchio G, Wang J P, Katine J A, Huai Y, Langer J, Galatsis K, Wang K L and Jiang H 2012 *ACS Nano* **6** 6115
[31] Hiroki M, Hitoshi K, Yoshishige S, Takayuki S, Kazumasa N, Yoshinori N, Koji T, Akio F, Alina M D, Koji A and Shinji Y 2013 *Appl. Phys. Express* **6** 113005
[32] Tsunegi S, Yakushiji K, Fukushima A, Yuasa S and Kubota H 2016 *Appl. Phys. Lett.* **109** 252402
[33] Kent A D, Özyilmaz B and del Barco E 2004 *Appl. Phys. Lett.* **84** 3897
[34] Lee K J, Redon O and Dieny B 2005 *Appl. Phys. Lett.* **86** 022505
[35] Houssameddine D, Ebels U, Delaet B, Rodmacq B, Firastrau I, Ponthenier F, Brunet M, Thirion C, Michel J P, Prejbeanu-Buda L, Cyrille M C, Redon O and Dieny B 2007 *Nat. Mater.* **6** 447
[36] Zeng Z, Finocchio G, Zhang B, Amiri P K, Katine J A, Krivorotov I N, Huai Y, Langer J, Azzerboni B, Wang K L and Jiang H 2013 *Sci. Rep.* **3** 1426
[37] Guo P, Feng J, Wei H, Han X, Fang B, Zhang B and Zeng Z 2015 *Appl. Phys. Lett.* **106** 012402
[38] Wang X, Feng J, Guo P, Wei H X, Han X F, Fang B and Zeng Z M 2017 *J. Magn. Magn. Mater.* **443** 239
[39] Quinsat M, Tiberkevich V, Gusakova D, Slavin A, Sierra J F, Ebels U, Buda-Prejbeanu L D, Dieny B, Cyrille M C, Zelster A and Katine J A 2012 *Phys. Rev. B* **86** 104418
[40] Tamaru S, Kubota H, Yakushiji K, Yuasa S and Fukushima A 2016 *Sci. Rep.* **5** 18134
[41] Gusakova D, Quinsat M, Sierra J F, Ebels U, Dieny B, Buda-Prejbeanu L D, Cyrille M C, Tiberkevich V and Slavin A N 2011 *Appl. Phys. Lett.* **99** 052501
[42] Slavin A and Tiberkevich V 2009 *IEEE. Trans. Magn.* **45** 1875
[43] Manfrini M, Devolder T, Kim J V, Crozat P, Chappert C, Van Roy W and Lagae L 2011 *J. Appl. Phys.* **109** 083940
[44] Zhang X, Chen H H, Zhang Z and Liu Y 2018 *J. Magn. Magn. Mater.* **452** 458
[45] Choi H S, Kang S Y, Cho S J, Oh I Y, Shin M, Park H, Jang C, Min B C, Kim S I, Park S Y and Park C S 2015 *Sci. Rep.* **4** 5486
[46] Liu Y and Zhang Z 2013 *Sci. Chin. Phys. Mech. Astron.* **56** 184
[47] Li Z, Zhang S, Diao Z, Ding Y, Tang X, Apalkov D M, Yang Z, Kawabata K and Huai Y 2008 *Phys. Rev. Lett.* **100** 246602
[48] Sankey J C, Cui Y T, Sun J Z, Slonczewski J C, Buhrman R A and Ralph D C 2008 *Nat. Phys.* **4** 67
[49] Kubota H, Fukushima A, Yakushiji K, Nagahama T, Yuasa S, Ando K, Maehara H, Nagamine Y, Tsunekawa K, Djayaprawira D D, Watanabe N and Suzuki Y 2008 *Nat. Phys.* **4** 37
[50] Zhu W, Zhang Z, Zhang J and Liu Y 2015 *SPIN* **05** 1550003
[51] Covington M 2005 *Science* **307** 215
[52] Lee K J, Deac A, Redon O, Nozieres J P and Dieny B 2004 *Nat. Mater.* **3** 877
[53] Ebels U, Houssameddine D, Firastrau I, Gusakova D, Thirion C, Dieny B and Buda-Prejbeanu L D 2008 *Phys. Rev. B* **78** 024436
[54] Wei Jin, Yaowen Liu and Chen H 2006 *IEEE. Trans. Magn.* **42** 2682
[55] Chen H H, Zhang Z, Chang C R and Liu Y 2017 *J. Appl. Phys.* **121** 013902

[56] Chen H H, Zhang Z, Liu Y and Chang C R 2015 *IEEE. Trans. Magn.* **51** 1401104
[57] Seki T, Mitani S, Yakushiji K and Takanashi K 2006 *Appl. Phys. Lett.* **89** 172504
[58] Lee O J, Pribiag V S, Braganca P M, Gowtham P G, Ralph D C and Buhrman R A 2009 *Appl. Phys. Lett.* **95** 012506
[59] Liu H, Bedau D, Backes D, Katine J A, Langer J and Kent A D 2010 *Appl. Phys. Lett.* **97** 242510
[60] Rahman M T, Lyle A, Amiri P K, Harms J, Glass B, Zhao H, Rowlands G, Katine J A, Langer J, Krivorotov I N, Wang K L and Wang J P 2012 *J. Appl. Phys.* **111** 07C907
[61] Rowlands G E, Rahman T, Katine J A, Langer J, Lyle A, Zhao H, Alzate J G, Kovalev A A, Tserkovnyak Y, Zeng Z M, Jiang H W, Galatsis K, Huai Y M, Amiri P K, Wang K L, Krivorotov I N and Wang J P 2011 *Appl. Phys. Lett.* **98** 102509
[62] Zhang H, Hou Z, Zhang J, Zhang Z and Liu Y 2012 *Appl. Phys. Lett.* **100** 142409
[63] Slonczewski J C 2002 *J. Magn. Magn. Mater.* **247** 324
[64] Chen H H, Zeng L, Zhao W and Liu Y 2018 *SPIN* **08** 1850013